International Journal of Extreme Manufacturing

Nano-additive manufacturing of multilevel strengthened aluminum matrix composites

OPEN ACCESS
IOP Publishing | IMMT
International Journal of Extreme Manufacturing
Int. J. Extrem. Manuf. 5 (2023) 015102 (11pp)
https://doi.org/10.1088/2631-7990/ac9ba2

Nano-additive manufacturing of multilevel strengthened aluminum matrix composites

Chenwei Shao[1,2,3,*], Haoyang Li[1], Yankun Zhu[2], Peng Li[4], Haoyang Yu[4], Zhefeng Zhang[2,3], Herbert Gleiter[5], André McDonald[1] and James Hogan[1,*]

[1] Department of Mechanical Engineering, University of Alberta, Edmonton T6G 1H9, Canada
[2] Shi-Changxu Innovation Center for Advanced Materials, Institute of Metal Research, Chinese Academy of Sciences, Shenyang 110016, People's Republic of China
[3] School of Materials Science and Engineering, University of Science and Technology of China, Hefei 230026, People's Republic of China
[4] nanoFAB Fabrication and Characterization Centre, University of Alberta, Edmonton T6G 1H9, Canada
[5] Institute of Nanotechnology, Karlsruhe Institute of Technology, Hermann-von-Helmholtz-Platz 1, Eggenstein-Leopoldshafen 76344, Germany

E-mail: chenweishao@imr.ac.cn and jdhogan@ualberta.ca

Received 23 May 2022, revised 27 July 2022
Accepted for publication 17 October 2022
Published 24 November 2022

Abstract

Nanostructured materials are being actively developed, while it remains an open question how to rapidly scale them up to bulk engineering materials for broad industrial applications. This study propose an industrial approach to rapidly fabricate high-strength large-size nanostructured metal matrix composites and attempts to investigate and optimize the deposition process and strengthening mechanism. Here, advanced nanocrystalline aluminum matrix composites (nanoAMCs) were assembled for the first time by a novel nano-additive manufacturing method that was guided by numerical simulations (i.e. the in-flight particle model and the porefree deposition model). The present nanoAMC with a mean grain size <50 nm in matrix exhibited hardness eight times higher than the bulk aluminum and shows the highest hardness among all Al–Al_2O_3 composites reported to date in the literature, which are the outcome of controlling multiscale strengthening mechanisms from tailoring solution atoms, dislocations, grain boundaries, precipitates, and externally introduced reinforcing particles. The present high-throughput strategy and method can be extended to design and architect advanced coatings or bulk materials in a highly efficient (synthesizing a nanostructured bulk with dimensions of $50 \times 20 \times 4$ mm^3 in 9 min) and highly flexible (regulating the gradient microstructures in bulk) way, which is conducive to industrial production and application.

Supplementary material for this article is available online

Keywords: high-throughput fabrication, bulk nanoAMC, low-temperature additive manufacturing, multi-level strengthening

* Authors to whom any correspondence should be addressed.

2631-7990/23/015102+11$33.00

1. Introduction

In order to meet the continuing increase in demand for high-tech fields (e.g. super speed vehicle, planetary rover, and bathyscaph), much effort has been implemented towards the development of advanced aluminum alloys or aluminum matrix composites (AMCs) [1, 2]. Generally, metals or alloys can be strengthened by introducing more grain boundaries (GBs) via grain refinement. But the high density of GBs provides a strong driving force for grain coarsening accompanied by property degradation. Recently, researchers found that nanometer-sized grains in copper and nickel produced from plastic deformation at low temperatures exhibit both notable thermal and mechanical stability below a critical grain size (commonly less than 70 nm) [3]. However, it is still difficult to reduce the grain size to the nanoscale (less than 100 nm) by currently known methods to rapidly synthesize Al alloys and their derivatives in bulk or coating forms. This is a consequence of the high atomic diffusivity in Al when they are exposed to elevated temperatures or mechanical loading [4]. Besides modification of Al matrix, alumina (Al_2O_3) is widely used as the particulate reinforcement in Al alloy, forming the putative AMC, because undesirable phases (e.g. Al_4C_3, Al_3Ti, and AlB_2 precipitates) are not produced in such material. However, defects can inevitably occur during the fabrication of Al–Al_2O_3 composites through traditional metallurgical processes (e.g. voids formed because of the difference in the matrix-particle coefficient of thermal expansion, difference in the rate of volume change, and poor wettability of Al_2O_3 particle in the Al matrix). Thus, pores are generally found in AMCs with high Al_2O_3 content, and this results in degradation of the mechanical properties (e.g. hardness, yield and ultimate strengths) of most Al–Al_2O_3 composites [5]. At present, Al nanocrystallization and porosity elimination are two major technical challenges in fabricating nanoAl–Al_2O_3 composites, especially at high Al_2O_3 content.

The research and development of advanced metal matrix composites (MMCs) is mainly the traditional trial-and-error mode, which is to solve the problems at the expense of long development cycle and high cost by dealing with individual cases according to the technical requirements of individual, small batch and multi-variety in the fields of aerospace and national defense. To this end, the idea of 'high-throughput preparation' (featured by high flux calculation design guiding the rapid optimization of material composition and preparation technology) was proposed [6], so as to achieve rapid optimization of material performance and realize the 'double half' in development cycle and cost. Significant developments have been achieved in recent years in high throughput design and preparation of low dimensional materials. Examples include numerical computation assisted diffusion-multiple approach [7], 'jet printing' synthesis [8], and selective laser cladding [9] strategies/technologies. While these studies have substantially advanced the fundamental science and technology of two-dimensional metallic functional materials (such as films and coatings), there is still much room for development in high throughput design and preparation of bulk nanostructured composites for broad industrial applications.

In this study, we extend the state-of-the-art in high-throughput fabrication of advanced AMCs by rapid and controlled synthesis of nanocrystalline Al matrix composites with minimal porosity and super high strength (proxied by high hardness). To the best of our knowledge, the composites from the present study exhibit the highest hardness among all Al–Al_2O_3 composites reported to date in the literature. These high-strength composites were designed by utilizing a multi-level strengthening strategy specialized for the cold spray additive manufacturing process, where numerical simulations were used to guide the process parameter optimization. The present preparation method (cryomilling and automated cold spraying) was featured with high fabrication efficiency and large dimensions in the sample size, and to be extended to other nanostructured MMCs (nanoMMCs) in the future and paves the way for their large-scale industrial application.

2. Experimental

2.1. Conceptual design and high-throughput construction of high-strength AMCs

Intermediate-polarization approach was selected to construct nanostructured matrix metal (improving the strength of matrix) and Solid approach was selected to construct MMC (adding the hard particles as many as possible while keeping the minimum porosity), and then nanostructured composite was synthesized with an emphasis on the high-throughput design (figure 1). Intermediate-polarization approach divided the grain size in powders to dozens of nanometers during the cryomilling process and then assemble these powders with Al_2O_3 particles together, which is able to construct the Al–Al_2O_3 composites with nanostructures. Specifically, cold spray was implemented as the synthesis technique after computational exploration of the powder pretreatment process and spraying parameters, in order to synergistically achieve self-strengthening of matrix metal and input of reinforcing particles as much as possible without introducing pores.

2.2. Materials and processes

Figure 2(a) schematically presents the cold spraying process for fabricating pure Al, Al alloys, and Al–Al_2O_3 composites. *Pure Al deposition*: Commercial 99% pure aluminum powders (SST-A5001, CenterLine, Ltd, Windsor, ON, Canada) prepared by gas atomization were sieved to achieve spherical powders with a size distribution of $\sim 53.3 \pm 4.9$ μm ($n = 5000$) using 40 μm and 60 μm sieves (figures 2(b) and (f)). The powders were mechanically milled at a rate of 200 rpm in a self-built ceramic/Al bi-layer vessel with stainless steel striking bars and stainless steel milling balls for 1 h under an ethyl alcohol or liquid nitrogen environment. Three milling temperatures were provided by the above environmental media: ethyl alcohol at room temperature ($\sim$25 °C); ethyl alcohol at

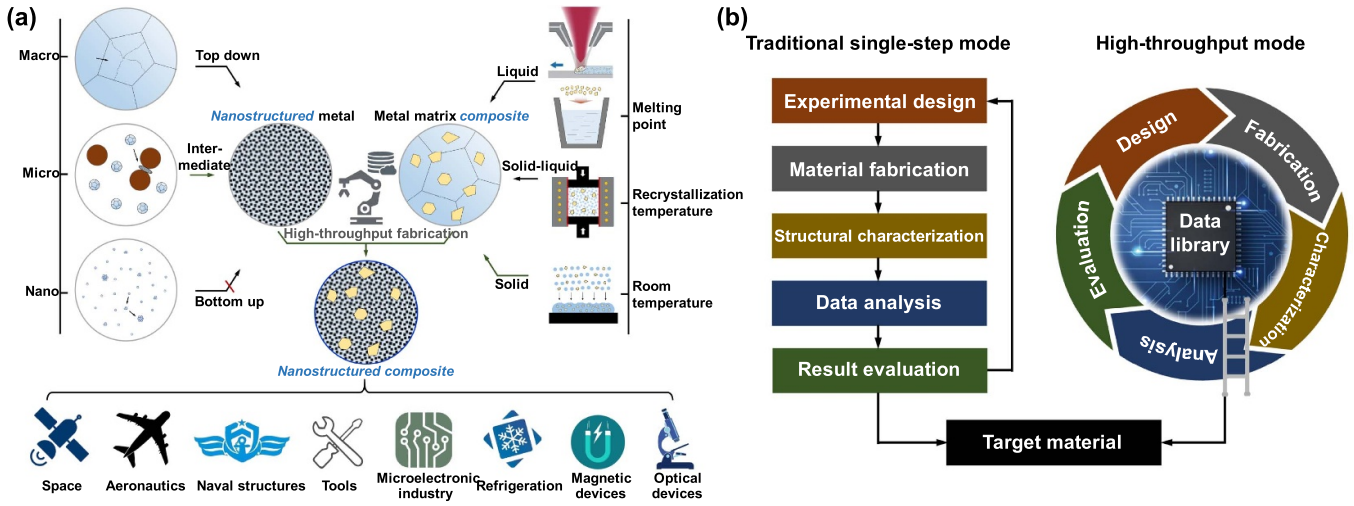

Figure 1. Overview of synthetic approaches and applications of nanostructured MMCs emphasized on the high-throughput design. (a) Base metal nanocrystallization includes top-down breaking the grains down in bulk material, bottom-up building the solid up from atomic scale units or nanoclusters, and reducing the structures in micron-scale (intermediate) particles before building them up. MMCs prepared by three (liquid, solid–liquid, and solid) approaches based on the state of matrix metal during forming process, including laser cladding/additive manufacturing, casting/impregnating, powder metallurgy, and depositing. Nanostructured composites show potentially structural and functional applications. (b) Comparison of two routes of new material development.

−100 °C, where liquid nitrogen was intermittently introduced into the alcohol to maintain the thermometer reading around −100 °C; and liquid nitrogen at −196 °C, where liquid nitrogen was continuously introduced into the vessel during milling to ensure complete immersion of the powders. Note that lowering the milling temperature helps reducing the grain size in powders (and finally the reduced grain size in deposited alloy/composite), because plastic deformation would be generally restrained at low temperature for metals. Stainless steel balls with 6 mm diameter were used as the grinding media and the ball-to-powder weight ratio was 20:1 for each milling operation. The thermometer is protected by a wire mesh from the impact of milling ball and an outlet channel is designed for monitoring the liquid level in ceramic vessel. An example of the powder morphology after milling in the liquid nitrogen is displayed in figures 2(c) and (g). The powders were then filtered from the ethyl alcohol or liquid nitrogen slurry after milling, and heated at 90 °C in a fume hood for 24 h to obtain dry powders for further cold spray deposition. These deformed powders were again sieved to get lamellar powders with maximum diameters between 80 μm and 300 μm. The sieved spherical/lamellar powders were then ready for subsequent cold spraying to fabricate the pure Al deposit with tailored grain sizes. *Al 6061 deposition*: commercial Al 6061 (with compositions: Mg 1.0%, Si 0.60%, Cu 0.28%, Cr 0.20%, Al balance) were melted and then gas atomized to obtain the corresponding alloy powders. The Al 6061 powders were ready for cold spraying after sieving, milling, filtering, drying, and secondary sieving processes, similar to which were applied in for pure Al. *Al–Al_2O_3 deposition*: 99.5% pure alumina (α-Al_2O_3) powders (Amdry 6060, Oerlikon Metco (Canada) Inc., Fort Saskatchewan, AB, Canada) prepared by a fusing and crushing process were sieved to a particle size distribution of ~38.7 ± 3.9 μm (n = 5000). An image of the powders after crushing and sieving are displayed in figures 2(d) and (h). These Al_2O_3 powders were then mixed with as-gas atomized or milled pure Al or Al 6061 powders at various mass ratios, respectively (i.e. powder blends of Al-30% Al_2O_3, Al-60% Al_2O_3, Al-90% Al_2O_3, Al 6061-30% Al_2O_3, Al 6061-60% Al_2O_3, and Al 6061-90% Al_2O_3). Powder mixing was performed in a rotated cylinder of 20 mm diameter at 20 RPM for 30 min. These powder blends were then ready for subsequent cold spraying to fabricate the Al–Al_2O_3 composites. Figures 2(e) and (i) shows the macro and micro 3D morphologies of an Al–Al_2O_3 composite cold sprayed using the Al-90% Al_2O_3 powder blend.

Shown at the bottom of figure 2(a) is the schematic of the automated cold spray system setup used in this study. All of the depositions of the pure Al, Al alloys, and Al–Al_2O_3 composites were performed using a portable cold spray system operating at low pressure (1 MPa gage or 150 psig maximum) (SST series P, CenterLine, Ltd, Windsor, ON, Canada). The cold-spray nozzle with a 6.4 mm exit diameter and 120 mm length was attached to a robot (Motoman HP-20, Yaskawa Electric Corp., Waukegan, IL, USA) to allow for control and repeatability of the deposition. The air temperature was set to 25 °C (for the nanocrystalline Al, Al alloy and nano Al based AMCs deposition) or 375 °C (for the other depositions) and the pressure was 90 psig. The nozzle traverse speed was set to 15 mm s^{-1} (as-gas atomized powders and their powder blends) or 5 mm s^{-1} (milled powders and their powder blends) with a stand-off distance (i.e. the distance between the substrate and the nozzle) of 10 mm for deposition. The deposition process was repeated several times (layer by layer) to fabricate the bulk deposits with dimensions of 50 × 20 × 4 mm^3. A volumetric powder feeder (5MPE, Oerlikon Metco, Westbury, NY, USA) was used to disperse and mix the powders further and transport them through the nozzle. Argon was used as the carrier gas in

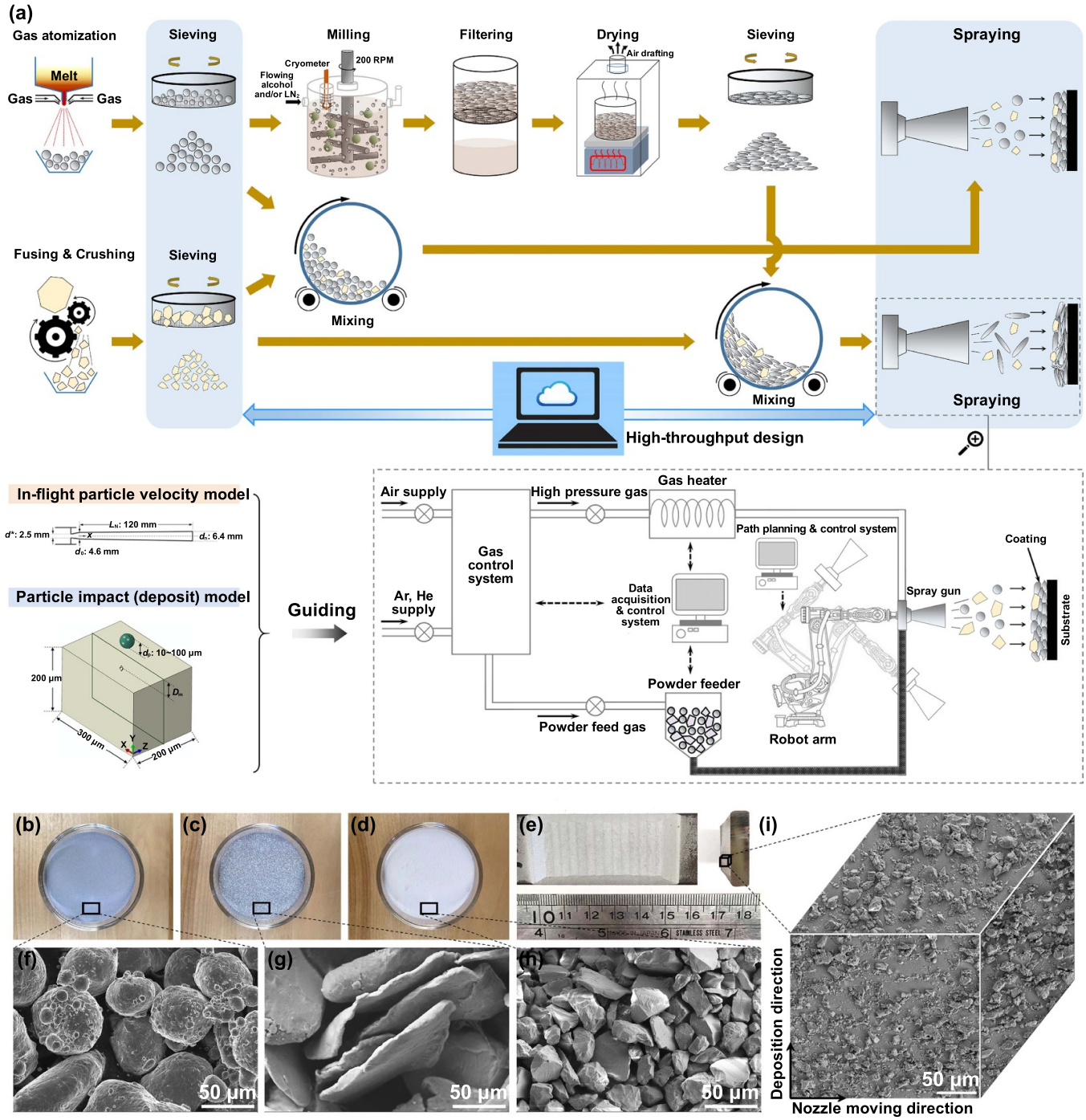

Figure 2. Material and preparation. (a) Schematic illustration of the fabrication process for nanocrystalline Al–Al_2O_3 composites pursued in this study. (b)–(i) Macroscopic and microscopic observations of powders used in cold spray composite deposition. (b), (f) Spherical Al powder before milling; (c), (g) Al powder after milling in the liquid nitrogen environment; (d), (h) irregularly shaped Al_2O_3 powder; (e), (i) a typical Al–Al_2O_3 composite prepared by cold spraying.

the powder feeder, which was fed into the cold-spray system at a pressure of 60 psig, and all the powders were fed at a rate of 60 flow meter reading. The substrate used was a 5 mm thick commercial 6061 Al alloy plate that was pre-roughened using #24 alumina grit media in a high pressure blasting machine (Manus Abrasive Systems, Inc., Edmonton, AB, Canada) to enhance the adhesion and deposition efficiency of the cold sprayed coatings.

2.3. Microstructure examination and mechanical tests

Microstructures, including the powder morphology, reinforcement Al_2O_3 particle distribution, precipitate and grain size distribution, and crystal orientation in the Al or Al alloy matrix, were analyzed by using a field-emission scanning electron microscope (SEM) (Sigma, Zeiss, Oberkochen, Baden-Württemberg, Germany) operated at 20 kV equipped

with energy dispersion spectroscopy (EDS) and electron backscatter diffraction (EBSD) capabilities. The AZtec analysis software was used to perform the EDS and EBSD analysis (AZtecOne and AZtecCrystal, Oxford instruments, Abingdon, Oxfordshire, United Kingdom) and obtain information on the elemental distribution, and lattice distortion and grain orientation, respectively. Before the SEM observations and analysis, samples were electro-polished in a solution of $HClO_4$:C_2H_5OH = 1:9 (vol.) under a voltage of 12.5 V for 60 s, in order to produce a strain-free and smooth surface after mechanical grinding. For the observations of the deformed powder morphology in the deposited coatings, particle splats were revealed by electrolytically etching using a 3 vol.% solution of fluoroboric (HBF_4) acid at room temperature and 12 V for 8 s. Samples prepared for transmission electron microscopy (TEM) investigations were all spark-cut from the bulk deposits from a section parallel to the deposition direction with an original thickness of 500 μm. The resulting thin section was ground mechanically to $\sim$10 μm (for Al or Al alloy) or $\sim$30 μm (for Al–Al_2O_3 composites) in thickness, and then was further polished to be electron transparent by a Ga focused ion beam cutting in a helium-ion microscope (from $\sim$10 μm to $\sim$50 nm) (ORION NanoFab, Zeiss, Oberkochen, Baden-Württemberg, Germany) or low energy Ar Ion in a broad ion beam polishing system (from $\sim$30 μm to dozens of nanometers) (EM RES102, Leica Microsystems, Wetzlar, Hesse, Germany) at room temperature. Most TEM or high resolution TEM observations were carried out using a JEOL JEM-ARM200CF S/TEM operated at an accelerating voltage of 200 kV with a cold field emission gun, except for the nanocrystalline samples which were observed using a FEI Tecnai T12 TEM operated at a relatively low accelerating voltage of 120 kV in an attempt to reduce the influence of the electron beam on the samples.

The hardness was carried out using a micro hardness tester (VH1202, Buehler Wilson, Lake Bluff, Illinois, USA) fitted with a Vickers indenter. The load was 500 g with a dwell time of 10 s. Most hardness tests were performed with the loading direction parallel to the *X* direction (orthogonal to the deposition direction and nozzle moving direction), except for those tested in *X, Y, Z* three directions. Each test was performed at room temperature and was repeated nine times ($n = 9$). Room temperature uniaxial compression tests were conducted at a constant strain rate of 1×10^{-3} s^{-1} using an Instron 3365 testing machine equipped with a Promon U750 high speed camera and a VIC 900170WOF LED laser light guide for illumination. Before testing, an airbrush with a 0.15 mm diameter nozzle was used to produce a fine speckle pattern (i.e. 5–10 pixels per speckle) on the specimen surface for digital image correlation (DIC) measurements. DIC analysis was performed using VIC-2D (v6 2018) software (Correlated Solutions Irmo, SC, USA).

3. Results and discussion

The proposed technical route was systematically validated on various cold sprayed materials, ranging from cold-sprayed pure Al to Al alloys, and finally to AMCs, as detailed in the section 2. In the next three subsections, the individual Strategies will be explored independently with controlled variables (i.e. initial powders morphology and fabrication conditions), and the following subsection presents a synergistic application with multi-level strengthening. Lastly, we discusses the feasibility of extending the proposed low-temperature additive manufacturing method to large-scale industry applications.

3.1. Rapid construction of nanocrystalline matrix metal (strategy I)

Grain size refinement, which can be technically achieved by plastic deformation or electrochemical deposition methods, has been widely recognized as an important strengthening mechanism. However, the extent of enhancement in strength (commonly there would be a large improvement in strength only if the grain size is reduced to less than 1 μm [10]) and rigorous processing conditions (e.g. severe plastic deformation at liquid nitrogen temperature [11]) by traditional methods are not practical for current industrial application. In this study, a high-efficiency additive manufacturing method incorporating temperature-controlled milling and automated cold-gas dynamic-spray processes was developed for synthesizing the Al or Al alloy matrices with various grain sizes, as introduced in the section 2. Using these approaches, four bulk pure Al (overall dimensions: 50 $\times$ 20 $\times$ 4 mm^3) with a deposited grain size of 4.9 $\pm$ 2.5 μm (figure S1(a)), 1.6 $\pm$ 1.1 μm (figures S1(b) and (c)), 222.4 $\pm$ 75.6 nm (figure S1(d)), and 43.1 $\pm$ 12.4 nm (figure 3(a)) were synthesized, respectively. At the powder boundaries of the deposit, the grain size is even smaller than that in the powders (e.g. less than 10 nm at boundaries compared to $\sim$200 nm in powders (figure 3(b)). In the grains with sizes larger than 1 μm, dislocation tangles were universally found (figure S1(c)). Finally, the relationship of hardness vs grain size for the present bulk pure Al are displayed in figure 3(c), and these are compared with the data of other pure metals from the literature. In figure 3(c), the hardness of present cold-sprayed Al was improved from 0.34 $\pm$ 0.03 GPa to 1.13 $\pm$ 0.08 GPa when the grain size is reduced from 4.9 $\pm$ 2.5 μm to 43.1 $\pm$ 12.4 nm.

The improvement in hardness caused by reducing the grain size indicates the effectiveness of the current strategy, which also follows the Hall–Petch prediction. By comparing with other pure metals, the pure Al fabricated in this study shows less improvement in hardness with respect to the grain sizes, and this can be a consequence of the higher stacking fault energy in Al. Like other metals with low melting points (e.g. Mg), it is generally challenging to further refine or maintain pure Al grains when their sizes are reduced to a few nanometers due to atomic diffusivity, especially at relatively high temperatures. High atomic diffusivity makes the structure and strength of metals unstable when they are exposed to mechanical loading, which limits the minimum grain size achievable in pure Al powders after the milling process. However, the present minimum grain size in bulk pure Al is much smaller than that achieved by the top-down approach (e.g. dynamic

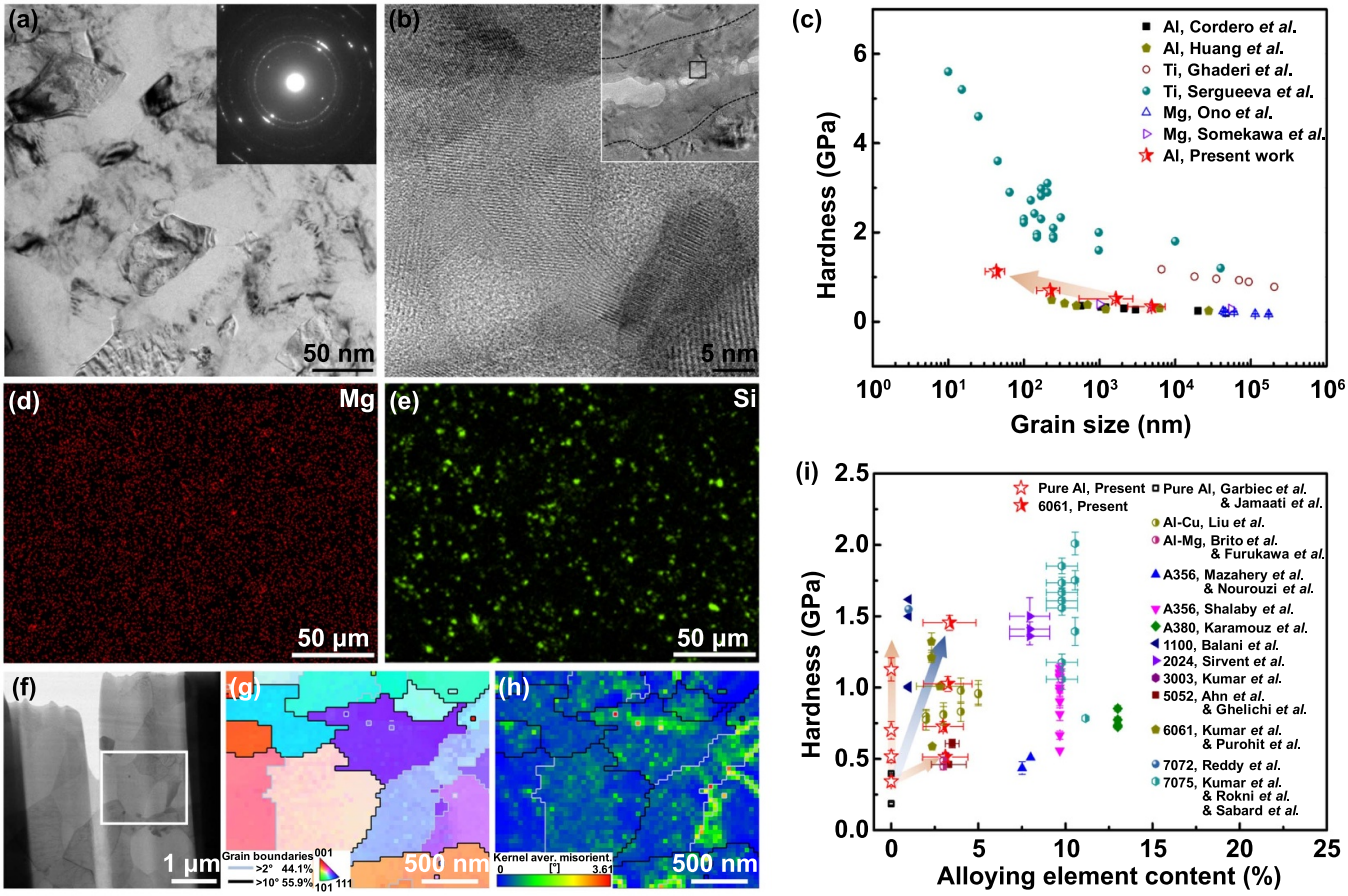

Figure 3. (a)–(c) Grain refinement (to nanoscale) via low-temperature milling and cold spraying processes. (a) Typical TEM image showing nanosized grains in a deposited Al. Inset shows (a) corresponding selected area electron diffraction (SAED) pattern. (b) High-resolution TEM image of the nanostructure at powder/powder boundary of the as-prepared Al. Inset is the corresponding lower magnification image with the boundary zone outlined by black dashed lines and the magnified area marked by a black box. (c) Correlation of grain size and hardness for the present cold sprayed Al deposits and other light metals from the literature. The closed points indicate hardness measured by hardness tests while the open points indicate yield strengths that were multiplied by a Tabor factor of 3 by compression or tension tests. (d)–(i) Solid solution atom and precipitate coupling with grain size. (d), (e) Elemental mappings of Mg and Si, (f) TEM image showing the microstructure of the alloy matrix, (g), (h) corresponding inverse pole figures (IPF) and kernel average misorientation (KAM) mappings characterizing the crystalline orientation in the white box of 'f', showing microstructure in cold sprayed Al 6061 using the powders milled at room temperature. (i) Correlation of alloying element content and hardness for the present cold sprayed Al and Al 6061, as well as other Al alloys from the literature. Note that the source where the hardness data come from can be found in data source section of supplementary information.

plastic deformation at liquid nitrogen temperature), where the minimum grain size was reported above 200 nm [12].

3.2. Solid solution atom and precipitate coupling with grain size (strategy II)

Alloying is another conventional strengthening mechanism through the interactions between solution atoms/precipitates and moving dislocations, which could potentially be beneficial to the promotion of strength. In this study, alloying is used in addition to grain refinement to further improve the strength of the Al matrix. To achieve solution and precipitate strengthening, Mg, Si, Cr, and Cu alloying elements (according to the commercial Al 6061 composition) were added to the Al melt pool during the gas atomizing process.

As an outcome, the final cold sprayed Al alloy contains homogeneously distributed Mg in the solid solution state (figure 3(d)), as well as precipitated Si (figure 3(e)). The EDS spectrum in figure S2(a) shows the alloying composition in the cold sprayed bulk material. In the Al matrix, numerous sub-GBs (occupying 44.1% of all the boundaries in the image) was introduced into the austenite grain when cold sprayed using the milled powders containing grains with an average size of 1.0 ± 0.6 μm, as shown in figures 3(f) and (g). Meanwhile, substantial crystal lattice distortion was found at some sub-GBs or in grains as an outcome of the alloying procedure, according to the kernel average misorientation (KAM) map (figure 3(h)). Finally, the hardness of alloyed Al (labeled as Al 6061) was improved by ∼50% compared with that of the pure Al prepared using non-milled powders in all indentation planes (figures S2(b) and (c)). The hardness of Al 6061 can be further enhanced from 1.13 ± 0.08 GPa up to 1.45 ± 0.05 GPa when coupling grain refinement in strategy I with alloy strengthening in strategy II (figure 3(i)).

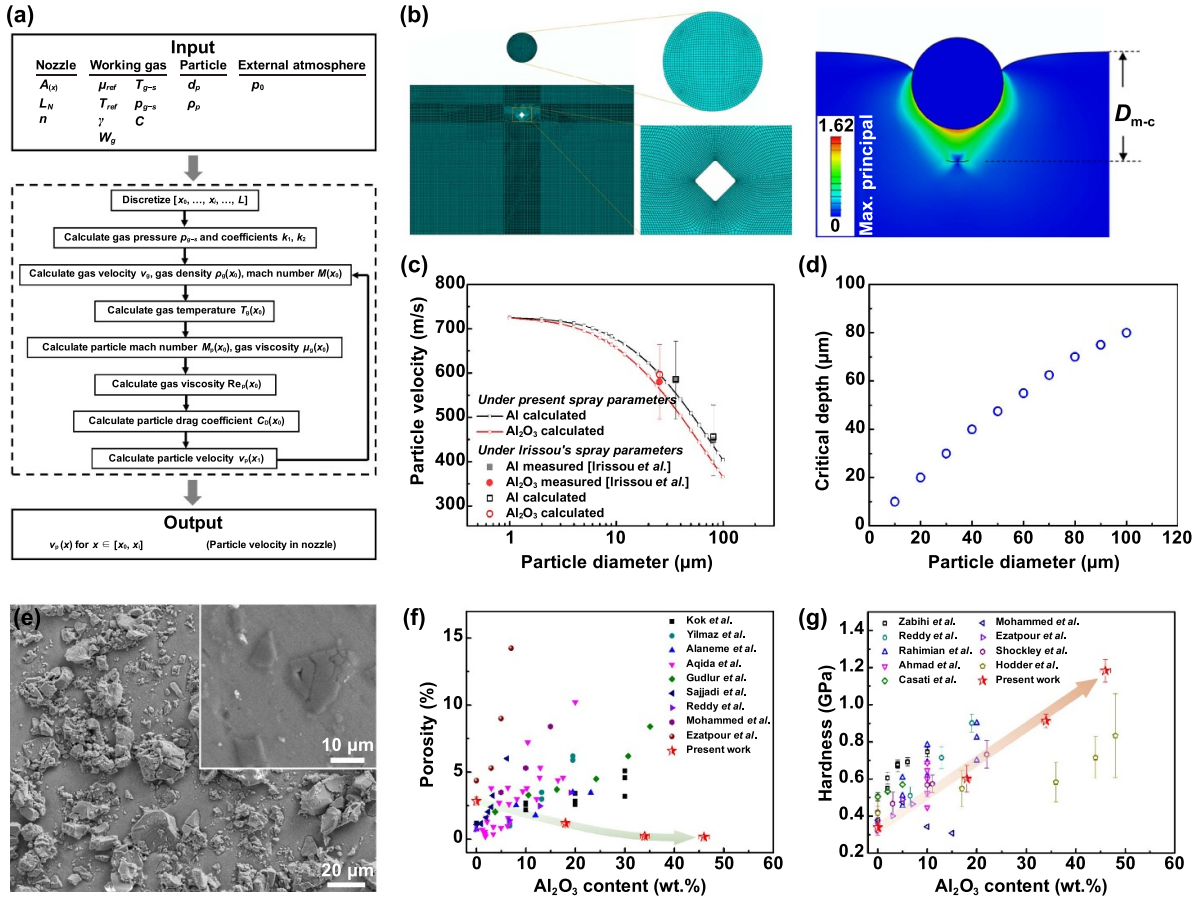

Figure 4. Porefree high-strength AMCs fabrication guided by numerical simulations. (a)–(d) Numerical approach for selecting optimized powder sizes for cold spray: (a) model flowchart for in-flight particle velocity evolution during cold spraying, (b) finite element methods (FEMs) simulation on spraying with impact of Al_2O_3 particle onto the Al matrix, (c) relationship between in-flight powder velocity and size after acceleration in the spray nozzle, (d) relationship between critical depth of embedded pore and Al_2O_3 particle size in the impact process. (e) Typical morphology of present Al-46% Al_2O_3 composite, showing minimal porosity and well bonded Al/Al_2O_3 interface. (f) Comparison of porosity between the present Al–Al_2O_3 composites and other Al–Al_2O_3 composites from the literature with the porosity versus Al_2O_3 content. (g) Correlation of Al_2O_3 content and hardness for the present composites and other Al–Al_2O_3 composites from the literature. (Please trace the hardness data through data source section of supplementary information).

This value is around the mean value in hardness of commercial Al 7075, but the present material shows less alloying element content (figure 3(i)), which may have benefits for resource sustainability.

3.3. High-throughput architecture of Al–Al_2O_3 composites with minimum porosity (strategy III)

The third Strategy used to enhance the strength (proxied through hardness) of the material was by introducing external hard reinforcing particles (Al_2O_3) while controlling the porosity, which was motivated by the Orowan strengthening mechanism. The influence of Al_2O_3 particles on strengthening and porosity was investigated in the pure Al based composites. To realize strategy III and inform on particle deposition conditions, a mathematical model describing the particle in-flight velocities in a cold spraying nozzle, followed by a finite element (FEM) simulation of the impact (deposition) process, were developed to guide the size selection for the matrix powder ($d_{p,Al}$) and reinforcement particle ($d_{p,Al2O3}$). Shown in figure 4(a) is the step-by-step procedure to modeling the particle in-flight velocity, where the particle velocity at the end point of the ith segment of the nozzle, $v_{p,i}$, is obtained by the following iteration processes, i.e.,

$$v_{p,i}^2 - v_{p,i-1}^2 = 2a_{p,i}L_N/n. \tag{1}$$

In equation (1), $v_{p,i-1}$ is the particle velocity at the starting point of the ith segment, L_N is the length of the nozzle, n is the number of segments inside the nozzle, and $a_{p,i}$ is the particle acceleration at the ith segment of the nozzle. The porefree deposition process is investigated by using an explicit dynamics analysis method through ABAQUS software platform (figure 4(b)). For the metal matrix, an experiment assisted isotropic hardening model was used to describe its gross plastic straining, where the Mises equivalent stress, $\bar{\sigma}$, satisfies the following equation:

$$\begin{aligned} &3G\left(\bar{e} - \Delta\bar{e}^{\mathrm{pl}}\right) - \bar{\sigma} = 0, \\ &\text{where} \quad \bar{e} = \sqrt{\frac{2}{3}\hat{e} : \hat{e}},\ \hat{e} = e^{\mathrm{el}}|_t + \Delta e \end{aligned} \tag{2}$$

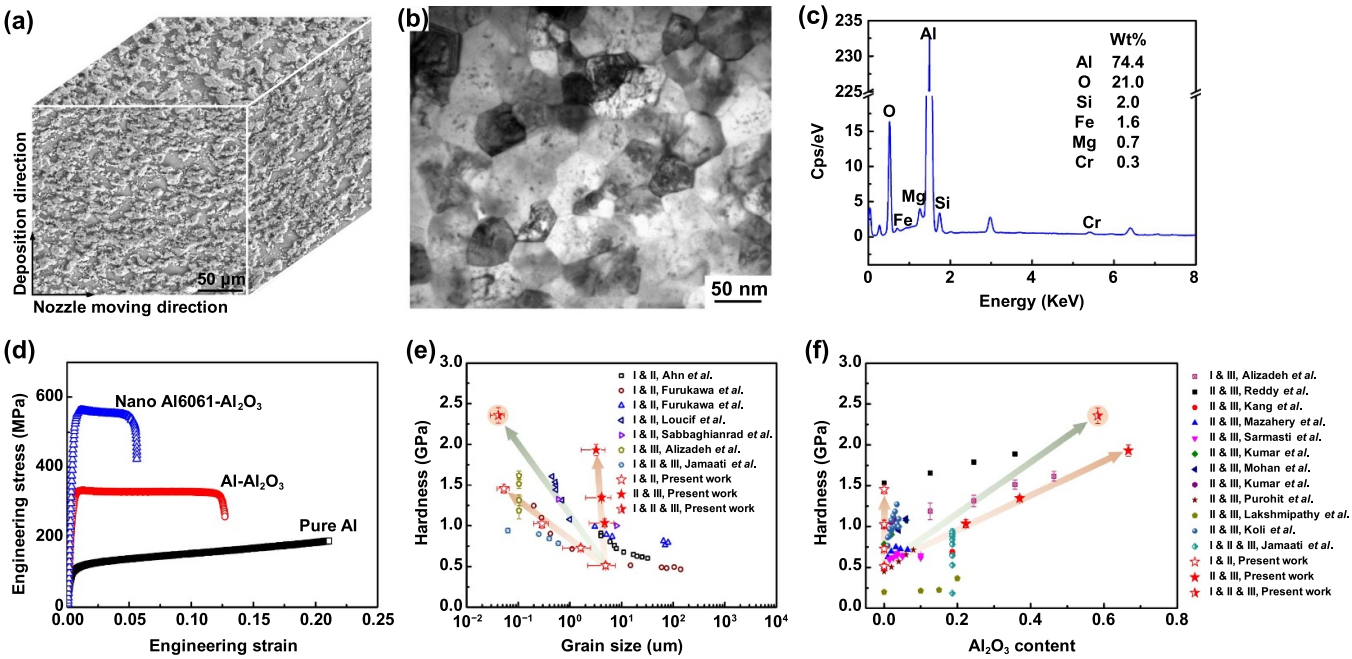

Figure 5. Multi-level strengthening in present nanocrystalline Al 6061–Al_2O_3 composite. (a)–(c) Microstructural information of the present composite designed by the synergistic strengthening strategy: (a) three-dimensional microstructure under SEM; (b) TEM image showing nanograined matrix; (c) the characteristic elemental x-ray energy peaks detected in the area containing Al matrix and Al_2O_3 particles. (d) Compression of stress–strain curves (in *Y* direction) of Al, Al–Al_2O_3, and nano Al 6061–Al_2O_3 under compression. (e), (f) Hardness of the present composites compared with other Al(–Al_2O_3) materials from the literature designed by two or three strengthening strategies: (e) Hardness versus grain size in matrix, (f) hardness versus Al_2O_3 particle content relationship for different strengthening strategies compared with those from the literature. (Please trace the hardness data through data source section of supplementary information).

In equation (2), G is the shear modulus, $\bar{e}$ and $\bar{e}^{\mathrm{pl}}$ are equivalent strain and equivalent plastic strain, $\mathbf{e}$ and $\mathbf{e}^{\mathrm{el}}$ are strain tensor and elastic strain tensor. Detailed introduction on the models and corresponding analysis on results are found in supplementary text and figures S3–S5.

The simulated results in figures 4(c) and (d) show that in order to obtain the AMC with sufficient interfacial adhesion and minimal porosity, two restrictions on powder size (i.e. $d_{\mathrm{p,Al}} < 70$ μm to ensure particle velocities greater than the critical velocity [13] for a successful deposition, and $2d_{\mathrm{p,\ Al2O3}} > d_{\mathrm{p,Al}}$ to make the pore closed in matrix) should be satisfied. At the same time, sufficient impact energy is needed to deform metal particles and promote adequate bonding at particle interfaces [13], thus, a larger powder size is preferred considering that the particle kinetic energy (E_{imp}) increases with increasing particle size for both Al and Al_2O_3 (figure S3(c)). From these considerations, spherical Al powders with powder sizes of $\sim$53.3 $\pm$ 4.9 μm and irregularly-shaped Al_2O_3 particles with sizes of $\sim$38.7 $\pm$ 3.9 μm were selected for cold spray fabrication of the present Al–Al_2O_3 composites. Deposition of irregularly-shaped particles has also been shown to have higher deposition efficiencies and better reinforcement effects [14] than with particles of spherical morphologies, thus justifying their selection here.

Informed by strategy III, three AMCs with Al_2O_3 content of 18.12 $\pm$ 0.81 wt.%, 34.04 $\pm$ 0.87 wt.%, and 46.02 $\pm$ 1.07 wt.% were prepared. The SEM micrograph shows that the Al and Al_2O_3 interfaces were well bonded (figure 4(e)), though larger areal fraction of pores were usually found in the matrices of AMCs with low Al_2O_3 content (figure S6). With the higher concentration of Al_2O_3 reinforcement particles, the porosity in the material was decreased from 2.84 $\pm$ 0.31 vol.% (Al) to 0.23 $\pm$ 0.04 vol.% (Al-34 wt.% Al_2O_3) or less (Al-46 wt.% Al_2O_3), as shown in figure 4(f). It is also noted that for almost all the conventional fabrication processes, such as casting and powder metallurgy, the porosity usually increases with increasing Al_2O_3 content in the composites, which reduces the strengthening effect from the addition of the Al_2O_3 particles. The cold spraying technique employed in this study eliminated this negative effect and produced the final composites with minimal porosity at high reinforcement particle content (figure S6). Finally, hardness measurements shown in figure 4(g) of the present Al-46 wt.% Al_2O_3 reached $\sim$1.2 GPa, which is among the highest value of all pure Al matrix Al–Al_2O_3 composites reported in the literature.

3.4. Synergistic application of strategies I, II, and III: multi-level strengthening

The present strategy emphasizes the multiscale strengthening involving all the above three mechanisms, and is able to prepare the nanograined metal matrix. With the knowledge obtained from the individualized design strategies (i.e. grain refinement, alloying, and particle dispersion), we then designed and synthesized Al–Al_2O_3 reinforced composites with a nanograined Al 6061 matrix through multi-level strengthening (see figures 5(a)–(c) for SEM, TEM, and EDS characterization). Figure 5(d) shows the typical compressive

engineering stress–strain curve of nano Al 6061–Al_2O_3 at room temperature, compared with that of pure Al and Al–Al_2O_3. From figure 5(d), the yield strength at 0.2% strain offset increased from approximately 102.4 MPa for pure Al to 557.0 MPa for nano Al 6061–Al_2O_3, and there was a transition of the work hardening rate from positive to negative. Damage and failure morphology observation on pure Al and nano Al 6061–Al_2O_3 after compression indicates that pure Al cracks inside first; while nano Al 6061–Al_2O_3 cracks along the shear plane, leaving some slipping traces on the side and obvious friction marks on the fracture (figure S7). Figure S8 shows the evolution of the axial strain spatial distribution for the as-sprayed pure Al and Al-46 wt% Al_2O_3 composite by DIC analysis. For pure Al, strain first concentrates in the center of the specimen and then extends to the surrounding regions (figure S8(a)). In comparison, a deformation band forms after yielding occurs in the as-sprayed Al–Al_2O_3 (figure S8(b)), indicating a shear-band-mediated fracture (i.e. the main fracture developed progressively by the initiation, growth, and coalescence of ductile microcracks).

To the best of our knowledge, the fabricated composite exhibited the highest hardness (2.36 $\pm$ 0.10 GPa) among all Al_2O_3 particle reinforced AMCs reported to date in the literature, as summarized in figures 5(e) and (f), regarding grain size and reinforcing particle content. The strengthening mechanisms presented here aims to include many meaningful microstructure strengthening factors that contribute to increasing the hardness in present AMCs (as summarized in figure S9). Specifically, it covers all the four classical strengthening mechanisms: solution strengthening, dislocation strengthening, interface strengthening, and precipitation/dispersion strengthening. In this study, strengthening by dislocation can be introduced through both cold spraying and milling. Since cold spraying is a deposition method wherein powder particles are accelerated in a supersonic gas jet to high velocities (300–1400 m s^{-1}) prior to impact on the substrate, metal powders (i.e. Al powder in the present work) will deform plastically upon impact to cause dislocation multiplication at these high impact velocities. In addition, dislocations will be introduced by severe plastic deformation during the milling process, accompanied by grain segmentation. As a result, the tangled dislocations (including the low-angle GBs) and newly formed GBs contribute to strengthening of the matrix crystal structures via dislocation–dislocation interaction and Hall–Petch effect, respectively. Meanwhile, the strengthening contribution from alloying elements and their distribution (e.g. solid solution strengthening from Mg atoms and precipitation strengthening from particle Si phase) further improves the hardness of the Al 6061 matrix. Lastly, the contribution from the Al_2O_3 reinforcement particles contributes to the multi-level strengthening resulting from the combination of Al/Al_2O_3 interface and Orowan-type strengthening mechanisms. Little texture was found in the cold sprayed Al 6061 (figure S10), though the powders were plastically deformed during the impact (figure S2(b)). Thus, the influence of texture or crystal orientation on mechanical properties can be neglected.

Finally, we note that the total strengthening effect is not the simple sum of individual strengthening factors. These strengthening mechanisms are also interconnected and can influence each other, which may result in additional strengthening beyond their individual contribution. For example, the austenite grains also experience strengthening due to formation of solid solution, tangled dislocations, and secondary phase particles, and this results in improved strengthening from grain refinement in Al 6061 alloy when compared to that observed in pure Al (figure 3(i)). It is also worth noting that unlike the multi-level strengthening mechanisms presented in this study, almost all traditional Al alloys or Al–Al_2O_3 composites from the literature were fabricated with only one or two strengthening strategies due to the restrictions from the fabrication method (figures 5(e) and (f)). It is often observed that the most desired microstructures can be obtained with only one certain strengthening strategy. For example, most Al or Al alloy shows a minimum grain size of over 100 nm (figure 5(e)), and the Al_2O_3 content in the AMCs was less than 25 wt.% (figures 4(g) and 5(f)). In another case, most alloy elements show limited solid solubility in aluminum, further adding these alloy elements may form various kinds of precipitations. Usually, an optimum content of alloy atoms added into the aluminum was found to be less than 10 wt.%, at which the composite exhibited good strength and plasticity match [15]. Therefore, there exists an upper bound for material enhancement using alloying alone, which further justifies our choice of incorporating other strengthening mechanisms (e.g. hard particle dispersion).

3.5. Prospects and applications

In our study, the present cryogenic milling with cold spraying fabrication process is proven to be applicable for rapid synthesis of bulk nanograined metals or alloys. We confirmed that a pure Al containing nanograins (<50 nm) with overall dimensions of 50 $\times$ 20 $\times$ 4 mm^3 can be built after 9 min of cold spraying. This technology is also applicable to construct heterogeneous and functionally-graded materials, which usually exhibit improved mechanical properties than single homogeneous materials [11]. Figure S11 shows an example of Al deposit with a bimodal structure (i.e. with μm-sized grains embedded inside a matrix of coarse (>5 μm) grains), which was cold-sprayed by using mixed powders containing gas atomized powders and milled powders. Little preferred crystallographic orientation (texture) or elongated grain is found in the sprayed Al matrices (see figures S10, 3(f), (g) and S1(a)–(d)), though the round powders are seriously deformed (figure S2(b)). Thus, there is little influence from the contribution of grain orientation or shape on the work hardening behavior, instead, the shape of deformed Al powders in the deposited bulk shows some impact on hardening. As shown in figures S2(c) and (d), the hardness is lower while the work hardening rate is higher in the deposition direction (*Z*) of bulk Al, compared to the other two directions (*X, Y*). Our most recent study show that it is the anisotropically distributed powder boundaries which contribute the anisotropies in hardness and

work hardening ability, due to the Hall–Petch relation from these boundaries. And the different loading conditions from hardness test and compressive test lead to the different trends in the anisotropy of mechanical properties. By modifying the powder microstructure (via milling) and/or chemical composition (via alloying) and controlling the blending ratio of powders/particles (via mixing), we successfully fabricated the Al or AMCs with various grain sizes, alloying elements, and particle content, with hardness ranging from ∼0.3 GPa to ∼2.4 GPa (figures 3–5). It is foreseeable that at least three kinds of graded materials can be synthesized with different and/or mixed powders by using the present method (figure S12). Thus, this method is conducive to fabricating high-performance alloys, because multilevel hierarchy of chemical and nanostructural heterogeneities is supposed to enable new combinations of properties and functionalities [16].

Noting that the present preparation method is essentially an additive manufacturing process, and the materials are *in situ* strengthened during the synthesis process. One of the advantages of this method is that it is free of a secondary working process (e.g. hydraulic pressing, hot extrusion, and equal channel angular pressing), which is often needed for strengthening the material prepared by traditional powder metallurgy methods. This methodological advantage can become critical especially when the processability of materials is poor. It may open the way to a new world of fabricating nanoglass alloys [17] characterized not only by new chemical compositions but also by new atomic arrangements and new properties. In addition, our recent work has shown that the strain concentration and macro cracks are easily formed in Al–Al_2O_3 composites with Al_2O_3 content exceeding 30% under compressive loading (figure S13), which raises difficulty in strengthening from traditional cold work process. Thus, the present preparation method can be applied to fabricate other high-strength materials with relatively low workability (e.g. hard alloys and metallic glass). It should also be noted that the 'nano-additive manufacturing' in this study mainly means fabricating solid bulk materials with nanostructures. Structural nano- and micro-additive manufacturing methods [18, 19] (commonly for porous materials) were developed and were then used to fabricate high-performance structural and functional materials in recent years, where materials' 'size effects' were utilized in the 3D architecture design. In the future, the two design philosophy, i.e. nanocrystallization in material and structural 3D micro-architecture, may be coupled in additive manufacturing to further improve the performance of present nanomaterials.

4. Conclusion

This study presented a high-throughput method for rapidly additive manufacturing the nanograined metals and nanoMMCs. As an application example, a series of bulk nanocrystalline Al and nanoAl–Al_2O_3 composites were prepared, whose hardness reaches as high as 2.4 GPa due to implementation of the multi-level strengthening strategy. Various particulate Al–Al_2O_3 composites with hardness ranging from 0.3 GPa to 2.4 GPa, as well as their mixture or gradient combinations, can be rapidly and accurately synthesized using the approaches proposed here. Meanwhile, the successful preparation of pore-free composites proves that the present numerical models can be used in optimizing cold spraying parameters. More importantly, the cryogenic milling and cold spraying method employed in this study may be easily adapted to current industrial processes and, hence, provides the potential for large-scale industrial fabrication of nanostructured materials.

Acknowledgments

Financial and technical support for this work was mainly received from InnoTech Alberta (Dr Gary Fisher), the Major Innovation Fund (MIF) Program, Imperial Oil, the Province of Alberta—Ministry of Jobs, Economy, and Innovation, and the Natural Science and Engineering Research Council of Canada. C S thanked the financial support from Youth Talent Promotion Project of China Association for Science and Technology (Grant No. YESS20200120), the Youth Innovation Promotion Association CAS (Grant Nos. 2022189), and Distinguished Scholar Project of Institute of Metal Research CAS (Grant No. 2019000179).

ORCID iD

Chenwei Shao https://orcid.org/0000-0001-7647-7719

References

[1] Sun W W, Zhu Y M, Marceau R, Wang L Y, Zhang Q, Gao X and Hutchinson C 2019 Precipitation strengthening of aluminum alloys by room-temperature cyclic plasticity *Science* **363** 972–5

[2] Shao C W, Zhao S, Wang X G, Zhu Y K, Zhang Z F and Ritchie R O 2019 Architecture of high-strength aluminum–matrix composites processed by a novel microcasting technique *NPG Asia Mater.* **11** 69

[3] Zhou X, Li X Y and Lu K 2018 Enhanced thermal stability of nanograined metals below a critical grain size *Science* **360** 526–30

[4] Meyers M A and Chawla K K 2009 *Mechanical Behavior of Materials* 2nd edn (Cambridge: Cambridge University Press)

[5] Sajjadi S A, Ezatpour H R and Torabi Parizi M 2012 Comparison of microstructure and mechanical properties of A356 aluminum alloy/Al_2O_3 composites fabricated by stir and compo-casting processes *Mater. Des.* **34** 106–11

[6] Curtarolo S, Hart G L W, Nardelli M B, Mingo N, Sanvito S and Levy O 2013 The high-throughput highway to computational materials design *Nat. Mater.* **12** 191–201

[7] Zhao J C, Jackson M R, Peluso L A and Brewer L N 2002 A diffusion-multiple approach for mapping phase diagrams, hardness, and elastic modulus *JOM* **54** 42–45

[8] Liu X *et al* 2012 Inkjet printing assisted synthesis of multicomponent mesoporous metal oxides for ultrafast catalyst exploration *Nano Lett.* **12** 5733–9

[9] Kang N, Coddet P, Wang J, Yuan H, Ren Z M, Liao H L and Coddet C 2017 A novel approach to *in-situ* produce functionally graded silicon matrix composite materials by selective laser melting *Compos. Struct.* **172** 251–8

[10] Cordero Z C, Knight B E and Schuh C A 2016 Six decades of the Hall–Petch effect—a survey of grain-size strengthening studies on pure metals *Int. Mater. Rev.* **61** 495–512

[11] Wang Y M, Chen M W, Zhou F H and Ma E 2002 High tensile ductility in a nanostructured metal *Nature* **419** 912–5
[12] Huang F and Tao N R 2011 Effects of strain rate and deformation temperature on microstructures and hardness in plastically deformed pure aluminum *J. Mater. Sci. Technol.* **27** 1–7
[13] Assadi H, Gärtner F, Stoltenhoff T and Kreye H 2003 Bonding mechanism in cold gas spraying *Acta Mater.* **51** 4379–94
[14] Weng L, Shen Y, Fan T X and Xu J Q 2015 A study of interface damage on mechanical properties of particle-reinforced composites *JOM* **67** 1499–504
[15] Rana R S, Purohit R and Das S 2012 Reviews on the influences of alloying elements on the microstructure and mechanical properties of aluminum alloys and aluminum alloy composites *Int. J. Sci. Res. Publ.* **2** 1–7
[16] An X H 2021 Structural hierarchy defeats alloy cracking *Science* **373** 857–8
[17] Gleiter H 2016 Nanoglasses: a new kind of noncrystalline material and the way to an age of new technologies? *Small* **12** 2225–33
[18] Vyatskikh A, Delalande S, Kudo A, Zhang X, Portela C M and Greer J R 2018 Additive manufacturing of 3D nano-architected metals *Nat. Commun.* **9** 593
[19] Hasan M, Zhao J W and Jiang Z Y 2019 Micromanufacturing of composite materials: a review *Int. J. Extreme Manuf.* **1** 012004